Universiteit Antwerpen

This item is the archived peer-reviewed author-version of:

Enhanced superconductivity of hydrogenated β_{12} borophene

Reference:
Soskic Bozidar, Bekaert Jonas, Sevik Cem, Milošević Milorad.- Enhanced superconductivity of hydrogenated β_{12} borophene
Nano letters / American Chemical Society - ISSN 1530-6984 - 24:40(2024), p. 12650-12657
Full text (Publisher's DOI): https://doi.org/10.1021/ACS.NANOLETT.4C03845
To cite this reference: https://hdl.handle.net/10067/2092010151162165141

uantwerpen.be
Institutional repository IRUA

Enhanced superconductivity of hydrogenated β_{12} borophene

Božidar N. Šoškić,[†,‡] Jonas Bekaert,[*,‡] Cem Sevik,[‡] and Milorad V. Milošević[*,‡]

†*Faculty of Natural Sciences and Mathematics, University of Montenegro, Džordža Vašingtona bb, 81000 Podgorica, Montenegro*

‡*Department of Physics and NANOlab Center of Excellence, University of Antwerp, Groenenborgerlaan 171, B-2020 Antwerp, Belgium*

E-mail: jonas.bekaert@uantwerpen.be; milorad.milosevic@uantwerpen.be

Abstract

Borophene stands out among elemental two-dimensional materials due to its extraordinary physical properties, including structural polymorphism, strong anisotropy, metallicity, and the potential for phonon-mediated superconductivity. However, confirming superconductivity in borophene experimentally has been evasive to date, mainly due to the detrimental effects of metallic substrates and its susceptibility to oxidation. In this study, we present an *ab initio* analysis of superconductivity in the experimentally synthesized hydrogenated β_{12} borophene, which has been proven to be less prone to oxidation. Our findings demonstrate that hydrogenation significantly enhances both the stability and superconducting properties of β_{12} borophene. Furthermore, we reveal that tensile strain and hole doping, achievable through various experimental methods, significantly enhance the critical temperature, reaching up to 29 K. These findings not only promote further fundamental research on superconducting borophene and its

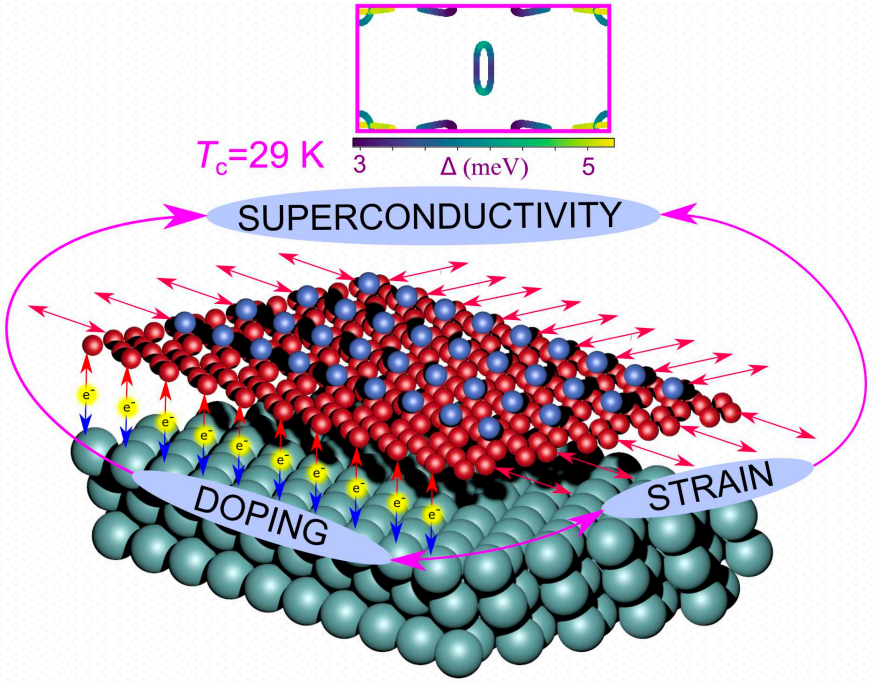

heterostructures, but also position hydrogenated borophene as a versatile platform for low-dimensional superconducting electronics.

Keywords

borophene, superconductivity, hydrogenation, strain, gating, *ab initio* calculations

With its intrinsic electron deficiency and more complex bonding nature than carbon,[1] boron ranks among the most chemically flexible elements, forming at least sixteen elemental bulk polymorphs,[2] as well as a plethora of cluster structures of diverse sizes,[3] including (quasi-)planar forms.[4] On that front, theoretical predictions[5,6] paved the way for the first experimental synthesis of two-dimensional (2D) boron structures, called borophenes, on a Ag(111) substrate in 2015.[7,8] These planar structures harbor a myriad of hexagonal voids with different concentrations and configurations.[9] The versatility of these borophenes is further demonstrated by their ability to be synthesized on a broad range of metallic substrates,[10–12] transferred onto other, nonmetallic substrates,[13] and ultimately isolated in

freestanding form via liquid-phase exfoliation.[14]

Borophenes exhibit a plethora of apposite physical properties, including mechanical compliance,[15,16] high optical transparency,[17] high hydrogen storage capacity,[18–20] ultrahigh thermal conductance,[21] the presence of metallic Dirac fermions,[22,23] and possible hosting of phonon-mediated superconductivity.[24–26] Hence, the potential utility of borophenes spans various applications, from electrodes in batteries[27] to catalysts for oxygen reduction[28] and detectors for gaseous substances.[29,30] However, practical applications may be hindered by borophene's susceptibility to oxidation in ambient conditions.[31–33] Surface hydrogenation emerges as a highly promising chemical passivation strategy, demonstrated to suppress oxidation of Si surfaces,[34] silicene,[35] and germanene.[36] A significant advancement in that respect took place in 2021 with the synthesis of several hydrogenated β_{12} borophene structures ("borophanes") on a Ag(111) substrate.[37] Borophanes exhibit remarkable stability in ambient conditions, with borophene readily recoverable through thermal desorption of the hydrogen adatoms.

In this work, we explore borophanes as hydrogen-based phonon-mediated superconductors, drawing inspiration from prior findings of high superconducting critical temperatures (T_c) in hydrogen-rich compounds.[38–40] This idea traces back to Ashcroft's seminal theoretical analysis in 1968, which predicted high T_c in highly compressed hydrogen, due to strong phonon-mediated superconducting pairing resulting from its low mass.[41] However, major practical challenges are posed by the immense pressure required for production of solid metallic hydrogen.[42,43] This has led to an alternative push for hydrogen-rich superconductors that are stable under ambient (pressure) conditions. Placing hydrogen adatoms onto low-dimensional materials has yielded a similar promise in this regard, as demonstrated for monolayers of MgB_2,[44] 2D metal carbides and nitrides (MXenes),[45] and elemental gallium monolayers dubbed gallenene.[46]

Contrary to earlier reports of a lack of T_c enhancement in some hydrogenated borophenes,[47,48] we find that hydrogenation of β_{12} borophene significantly boosts both its stability and super-

conducting properties. This discrepancy stems from the selection of the electronic smearing parameter, with our findings showing that a sufficiently small value (0.0025 Ry, compared with the commonly used 0.02 Ry[24,25,47,48]) is essential for accurate well-converged superconducting predictions (cf. Figure S8 in the SI). Furthermore, by employing fully anisotropic Migdal-Eliashberg theory, we provide detailed insight into the origins of the material's superconducting behavior on the atomic scale. Additionally, we uncover several experimentally feasible strategies (strain, carrier doping) to further boost borophane's superconducting performance, leading to T_c values up to 29 K.

As the first step in our investigation, we determine the structural properties of bare and hydrogenated β_{12} borophene, as shown in Figure 1(a). The bare crystal structure consists of a planar sheet of boron (B) atoms arranged in a triangular lattice, with the exception of a row of hexagonal hollows with a missing boron atom at their center. The remaining occupied central B sites act as electron donors, while the hollows themselves are electron acceptors, creating a unique "self-doping" mechanism. Furthermore, the structure belongs to space group *Pmmm* (No. 47), with different coordination numbers for the constituent boron atoms, influencing local electronic properties and their resulting reactivity, and enabling adsorption of hydrogen on different sites. Despite its inherent dynamical instability in the freestanding form, we achieve stabilization of β_{12} borophene through hydrogen adsorption, pinpointing the optimal adsorption site at the "bridge" position (H_{bridge}-β_{12}), characterized by the highest binding energy among all considered configurations, amounting to 3.39 eV.

In Figure 1(b), one observes that the bonding states (σ) of the in-plane B orbitals, composed of $s + p_{x,y}$ orbitals, are nearly fully occupied in the bare phase, with a gap of over 3 eV separating them from their antibonding counterparts (σ^*). The remaining electrons occupy the states composed of the out-of-plane B-p_z orbitals. On the other hand, our Bader analysis reveals that hydrogen extracts $0.5e$ from the borophene layer, thus altering the electronic band structure. Hydrogenation also changes the lattice symmetry, so that the H_{bridge}-β_{12} borophene structure corresponds to space group *Pmm2* (No. 25).

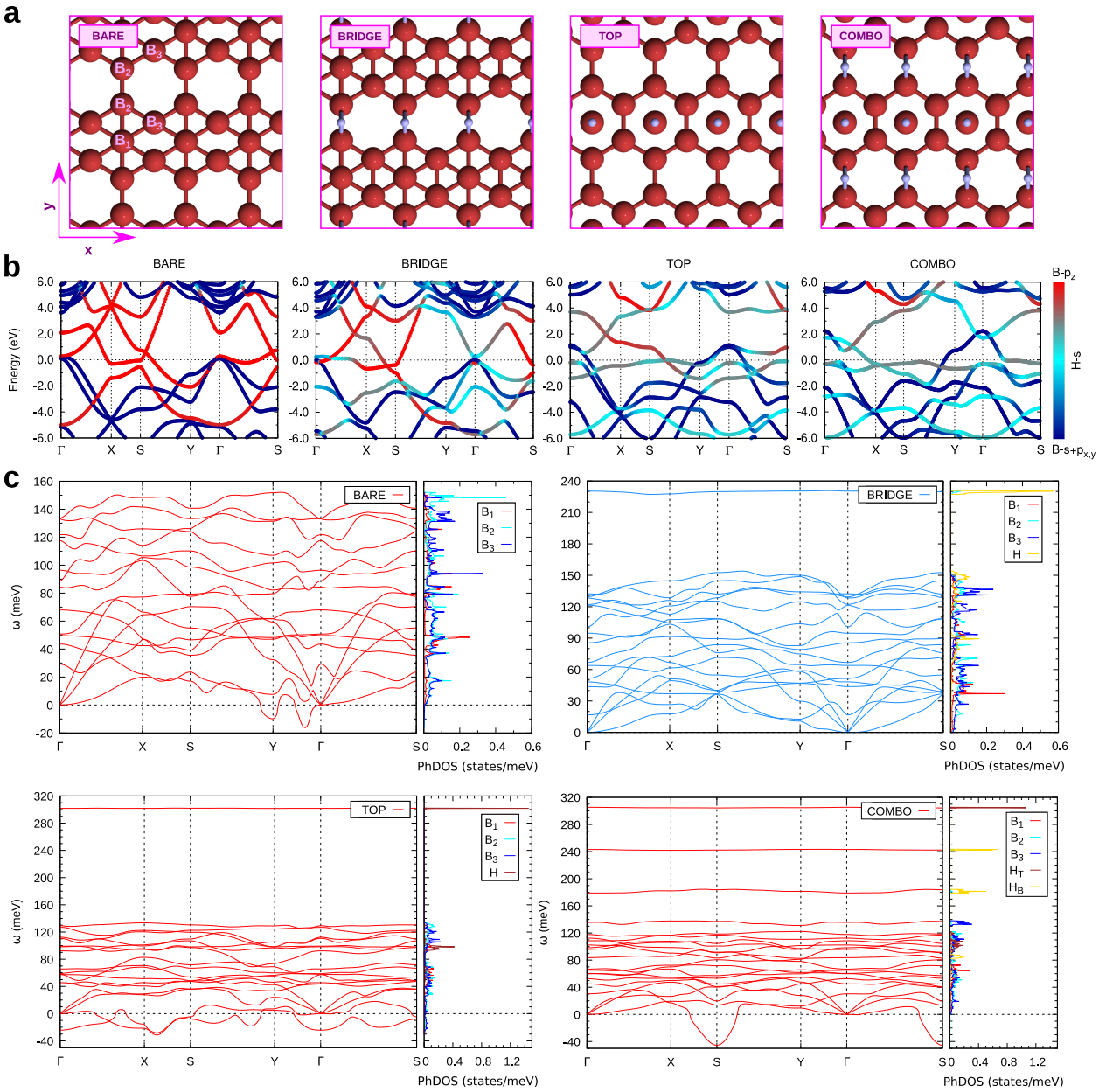

Figure 1: **Structural, electronic, and vibrational properties of bare and hydrogenated β_{12} borophene.** (a) Top views of the crystal structures of bare and hydrogenated borophene (bridge, top, and combo adsorption site), together with their (b) orbital-resolved electronic band structures, and (c) corresponding phonon dispersions and atom-resolved phonon density of states (phDOS).

The phonon band structure of the bare β_{12} borophene phase, obtained from our density functional perturbation theory (DFPT) calculations, displays a dynamical instability – see Figure 1(c). It arises mainly from the weak B_2–B_2 atom bond, resulting in unstable out-of-

plane phonon modes, as displayed in Figure S5 in the Supporting Information (SI). However, when hydrogen is adsorbed at the "bridge" site, this bond is reinforced, and a robust B_2–H–B_2 three-center bond is formed. This strengthened bond is responsible for the dynamical stability of this hydrogenated compound (see Figure 1(c)), in contrast with its bare electron-deficient form.

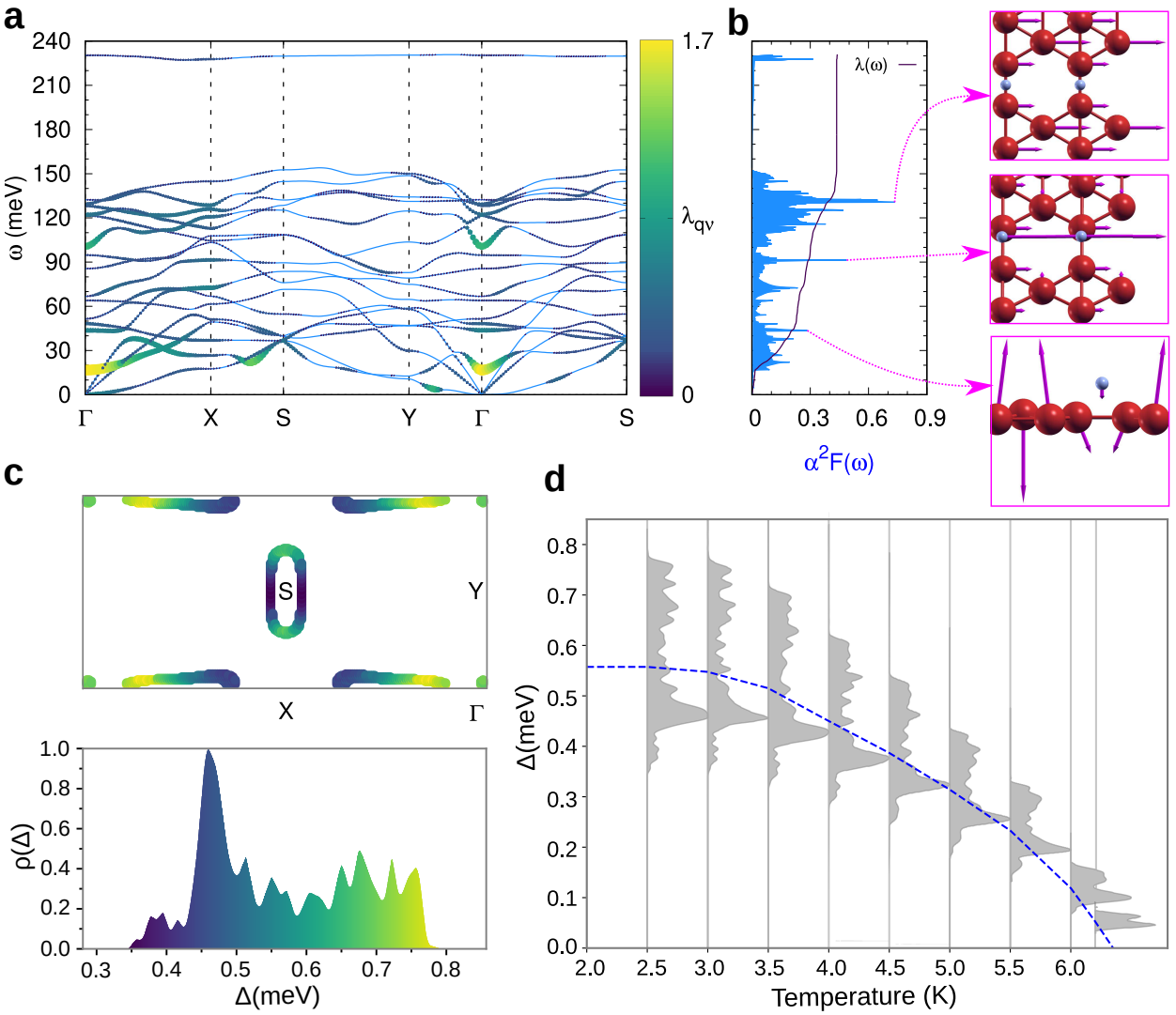

Figure 2: **Superconducting properties of H_{bridge}-β_{12} borophene, calculated with fully anisotropic Eliashberg approach.** (a) Phonon dispersion with the momentum-resolved electron-phonon coupling $\lambda_{\mathbf{q}\nu}$ indicated by colors. (b) The isotropic Eliashberg function, and phonon modes corresponding to peaks in the Eliashberg function. (c) The superconducting gap spectrum on the Fermi surface, calculated at 2.5 K, and the corresponding distribution $\rho(\Delta)$ with the color code. (d) The evolution of $\rho(\Delta)$ with temperature, including weighted averages (dashed blue line), yielding T_c^{aniso} of 6.3 K.

The other chief hydrogenated configurations that have been experimentally identified in Ref. 37 include the top site, and a combination of the top and bridge sites which we refer to as "combo", both depicted in Figure 1(a). Hydrogen on the top site of borophene leads to dynamical instability, exhibiting unstable phonon branches throughout the entire Brillouin zone (see Figure 1(c)), accompanied by pronounced structural buckling. In contrast, the dynamical instability of the "combo" configuration is characterized by an unstable phonon mode localized around the S point. It involves out-of-plane movement of the B_2 and H_{bridge} atoms along with in-plane movements of the B_3 and H_{top} atoms.

The electron deficiency of the "combo" configuration causes gapping between the B-π and π^* states (see Figure S13 in the SI). We thus found that adding electrons to this system so as to further fill up the π^* states achieves dynamical stability, in analogy to the dynamically stable bridge configuration where the π^* states are more occupied. Indeed, our simulations show that adding 0.1 e/B is required to stabilize the structure, the amount which the additional hydrogen atom has extracted from the borophene layer. By shifting the Fermi level, a good electronic balance between the partially filled σ and π^* states can be achieved, which is crucial for dynamical stability of the material. However, the values of the isotropically evaluated λ_{iso} and T_c^{iso} remain small, with superconductivity even vanishing for doping levels beyond 0.1 e/B (see Figure S15 in the SI). This is linked to the decreasing contributions of B_1-p_z, B_2-p_z and H-s states to the density of states at the Fermi level (E_F), while only contributions from B-σ states remain significant (see Table S2 in the SI). Generally, when comparing these "top" and "combo" configurations with the H_{bridge}-β_{12} structure, they do not harbor notable superconducting properties.

Let us now delve deeper into the vibrational and superconducting properties of the most promising candidate for superconductivity, namely the H_{bridge}-β_{12} borophene configuration. In Figure 2(a), we present its phonon band structure alongside the mode(ν)- and momentum($\mathbf{q}$)-dependent electron-phonon (e-ph) coupling ($\lambda_{\mathbf{q}\nu}$). The strongest coupling is found around Γ for phonon energy values of ~ 20 meV. This corresponds to the softened B_1 opti-

cal phonon mode. In Figure 2(b), the Eliashberg function reveals several significant peaks, with primary contributions stemming from two phonon modes. The first one corresponds to the in-plane and in-phase movement of B_1, B_2 and H (and slight in-plane and out-of-phase movement of B_3) at ∼90 meV. The second one – the highest peak overall – originates from the optical A_u phonon mode, stemming from the in-plane movement of B atoms at ∼130 meV. The resulting overall isotropic *e-ph* coupling constant amounts to $\lambda_{\text{iso}} = 0.44$, yielding a critical temperature of $T_c^{\text{iso}} = 4.0$ K using the McMillan-Allen-Dynes (MAD) formula.

To accurately assess the influence of hydrogenation on borophene's superconducting properties, we employ our first-principles results as input to solve the fully anisotropic Migdal-Eliashberg equations. Through this approach, we obtain the superconducting gap $\Delta(\mathbf{k})$ as a function of electron momentum $\mathbf{k}$ at the E_F, shown in Figure 2(c). The Fermi surface is composed of three sheets: (i) an ellipsoidal Fermi sheet located around the S point, with hybridized B-p_z and H-s character, (ii) an elongated sheet extending along Γ-X, where the character varies from purely B-p_z (close to Γ) to hybridized B-p_z/H-s further away from Γ, and (iii) a small circular sheet around Γ with purely B-σ character. The Fermi sheet around S hosts the lowest $\Delta(\mathbf{k})$ values (0.35 meV at 0 K), where the electronic character is purely B-p_z, and slightly higher values where the character is hybrid B-p_z/H-s. For the sheet along Γ-X, the lowest gap values (down to 0.43 meV) stem from hybridized B-p_z and H-s states, while the highest ones (up to 0.78 meV) stem from pure B-p_z states.

Nevertheless, the gap distribution $\rho(\Delta)$ (see Figure 2(c)) does not present separate domes, hence, its superconductivity is anisotropic single-gap in nature. Figure 2(d) shows the temperature evolution of $\Delta(\mathbf{k})$, obtained from solving the anisotropic Eliashberg equations for each temperature. This yields $T_c^{\text{aniso}} = 6.3$ K, the temperature where gap vanishes. Furthermore, to assess the contributions of the different chemical elements in H_{bridge}-β_{12} borophene, we also investigated the isotope effect. To this end, we renormalized the phonon frequencies according to the isotope masses and subsequently solved the anisotropic Eliashberg equations again. We found a stronger B isotope effect ($\alpha_{\text{B}} = 0.63$) compared with the H isotope

effect ($\alpha_{\mathrm{H}} = 0.05$), underscoring hydrogen's pivotal role in enhancing stability in bare β_{12} borophene while maintaining its intrinsic superconducting properties.

As a next step, we have considered the influence of lattice deformation on the superconducting properties of $\mathrm{H_{bridge}}$-β_{12} borophene. Applying strain to 2D materials is experimentally viable through e.g. the selection of a suitable substrate, or using a piezoelectric substrate, and has proven to be a successful route to tailor and enhance superconductivity in various 2D superconducting systems.[44,49] Given the strong anisotropy of β_{12} borophene, we applied the in-plane strain (ϵ) not necessarily equal in the x and y directions (see Figure 1(a)). We have considered values for ϵ_x and ϵ_y ranging from -5% (compressive) to $+5\%$ (tensile) strain, with a step size of 1% – yielding 121 strain combinations in total.

Considering first the effect of strain on bare β_{12} borophene, we found that it becomes dynamically stable under a biaxial tensile strain of $\epsilon_{x,y} = +3\%$, achieving a T_c^{iso} of 2.13 K, however, superconductivity is suppressed once the strain level reaches $\epsilon_{x,y} = +5\%$, due to a rapid decrease of the DOS at the E_F, contributed by the B-σ states (see Table S1 and Figure S7 in SI).

Upon hydrogenation, we found that hydrogen significantly stiffens β_{12} borophene due to its inherently high phonon frequencies, rendering it unable to sustain compressive strain. On the other hand, the phonon spectra remain stable for tensile strain up to $+5\%$ for the majority of strain combinations, as shown in Figure 3(a,b).

The figure reveals distinctive changes in λ_{iso} with applied strain, which can be attributed to the interplay of two effects. Firstly, in the absence of strain in the y direction, as ϵ_x increases, the p_z contributions from $\mathrm{B_1}$ and $\mathrm{B_2}$ atoms decrease, leading to a reduction of λ_{iso}. Conversely, when no strain is applied in the x direction, we observe an increasing contribution of σ states from $\mathrm{B_1}$ and $\mathrm{B_2}$ atoms as ϵ_y increases, leading to a distinct enhancement of λ_{iso}. Other strain combinations are governed by the interplay between these two elementary tendencies. The trend in λ_{iso}, driven by changes in interatomic charge densities, reveals that tensile strain along the y direction lengthens all B-B and B-H bonds as anticipated,

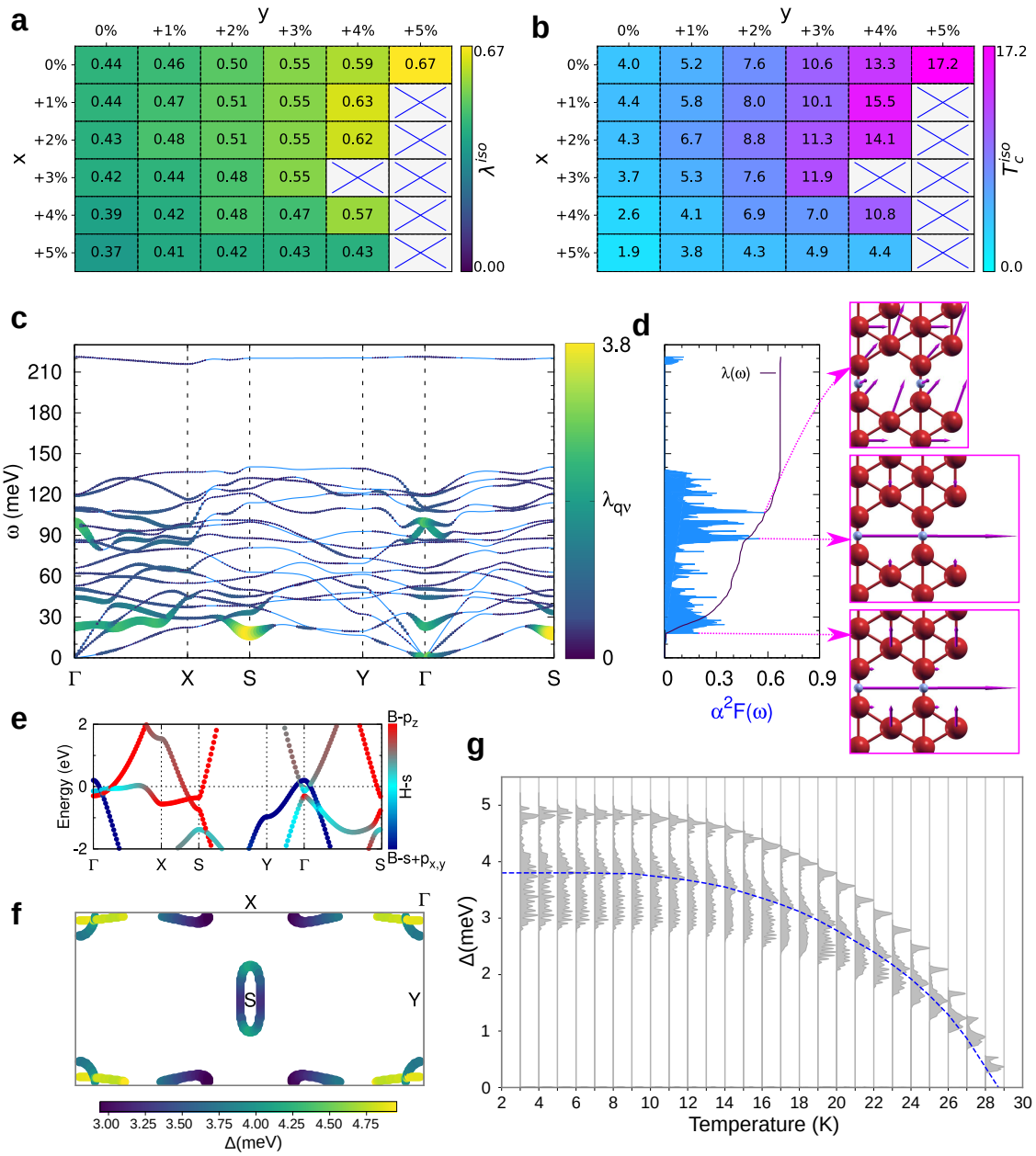

Figure 3: **Superconducting properties of H_{bridge}-β_{12} borophene under (anisotropic) in-plane tensile strain.** (a) The isotropic *e-ph* coupling, and (b) corresponding T_c^{iso} values for considered tensile strains along the two principal in-plane directions, with maximal values found for for uniaxial tensile strain of $\epsilon_y = 5\%$. For the latter optimal case, panel (c) shows the phonon dispersion with the momentum-resolved *e-ph* coupling $\lambda_{\mathbf{q}\nu}$ indicated by colors. (d) The corresponding isotropic Eliashberg function, and phonon modes corresponding to its selected peaks. (e) The corresponding orbital-resolved electronic band structure. (f) The superconducting gap spectrum on the Fermi surface, calculated at 3 K. (g) The evolution of $\rho(\Delta)$ with temperature, including weighted averages (dashed blue line), yielding $T_c^{aniso} = 28.6$ K.

whereas strain along the x direction compresses the B_2-B_2 bond to adjust for charge density changes, leading to increased phonon frequencies and reduced *e-ph* coupling (see Table S3 and S4 in SI). Furthermore, H_{bridge}-β_{12} borophene shows superior superconducting properties compared with its bare form under the same biaxial strain values (see Figure S7 in SI).

The above comprehensive analysis showed the H_{bridge}-β_{12} structure under a 5% uniaxial tensile strain in the y direction to be the best candidate for superconductivity, with higher strain values showing no further enhancement (see Figure S66 in SI). Its λ_{iso} reaches 0.67, with the corresponding highest T_c^{iso} of 17.2 K. The strongest $\lambda_{\mathbf{q}\nu}$ value occurs at the S point at low frequencies [see Figure 3(c)]. The corresponding mode is composed of out-of-plane movement of B_3 atoms and in-plane movement of B_2 and H atoms [see inset of Figure 3(d)]. The Eliashberg function in Figure 3(d) exhibits two more significant peaks. The first one occurs at ∼90 meV stemming from in-plane H (and slight out-of-phase B_3) movement, and the highest A mode at ∼110 meV, arising from in-plane B and slight out-of-plane H movement.

As shown in Figure 3(f), the Fermi surface exhibits strong anisotropy, prompting us to perform fully anisotropic Migdal-Eliashberg calculations to thoroughly characterize its superconducting properties. Within the ellipsoidal sheet located around the S point, $\Delta(\mathbf{k})$ originates from hybridized B-p_z and H-s states. Along Γ-X, the lower gap values stem from hybridized B-p_z and H-s states, while the highest values originate from the pure B-p_z state. Despite some changes in the composition of the Fermi surface, these characters and how they relate to the $\Delta(\mathbf{k})$ values are completely in line with the unstrained counterpart discussed before. Exhibiting a strongly anisotropic single-gap nature, the $\Delta(\mathbf{k})$ values reach up to 4.95 meV at 0 K, corresponding to an enhanced T_c^{aniso} value of 28.6 K, as shown in Figure 3(f).

Besides strain engineering, controlled charge doping is another established method to modulate the electronic properties of 2D materials, and can furthermore occur naturally as an additional effect of certain substrates. We have simulated spatially uniform doping as well as non-uniform field-effect transistor (FET) type-doping, within a single-sided gate

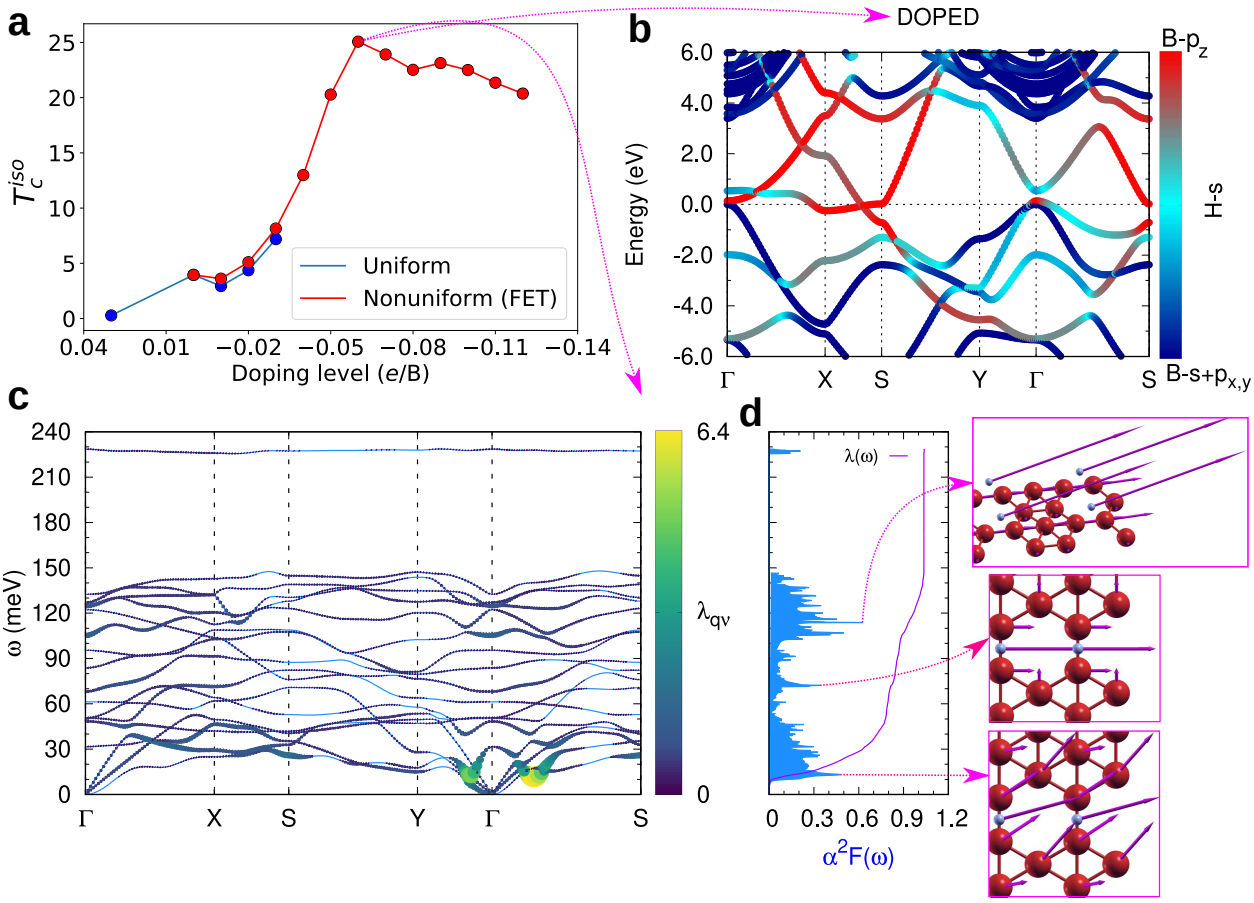

Figure 4: **Superconducting properties of H_{bridge}-β_{12} borophene under the influence of both uniform and non-uniform electron and hole doping.** (a) The dependence of T_c^{iso} on the doping level. The negative values correspond to hole doping as electrons are removed in this case. (b) The electronic band structure with the band character indicated by colors for 0.06 e/B hole doping. (c) The corresponding phonon dispersion with the momentum-resolved electron-phonon coupling $\lambda_{\mathbf{q}\nu}$ indicated by colors. (d) The isotropic Eliashberg function, and phonon modes corresponding to the main peaks in the Eliashberg function.

geometry (see SI for computational details).

As the first step, we found that the bare form of β_{12} borophene remains dynamically unstable upon both electron and hole doping. In contrast, for H_{bridge}-β_{12} borophene with a non-uniform hole doping level of 0.06 e/B, the structure is dynamically stable and T_c^{iso} reaches 25.1 K, as shown in Figure 4(a).

Since the electronic DOS at the E_F strongly affects λ_{iso}, and is readily altered by carrier doping, we investigated its effect on the superconducting properties. We found that the

DOS at E_F decreases (increases) with electron (hole) doping (see Table S5 and S6 in SI). Notably, the contribution of B-σ and B-p_z states increases upon hole doping, boosting λ_{iso} up to 1.04 (at 0.06 e/B). The largest $\lambda_{\mathbf{q}\nu}$ values stem from the softened A phonon mode along Γ-X at $\sim$10 meV, corresponding to in-plane movement of H atoms and rotating movement of B atoms [see Figure 4(c,d)]. The other two important peaks at higher frequencies in the Eliashberg function are due to the A_g phonon mode at $\sim$70 meV, stemming from in-plane B_2 and H (and slight out-of-phase B_3) movement, and the phonon mode at $\sim$110 meV corresponding to in-plane and in-phase movement of B_2 (slight in-plane and out-of-phase B_3) and out-of-plane movement of H atoms, as shown in Figure 4(d). Overall, our findings indicate that hole doping is an efficient mechanism to enhance λ_{iso}, next to the tensile strain. However, when applied simultaneously, the combined effect of strain and doping reduces λ_{iso} and T_c^{iso} due to the decreased contribution of B-σ states at E_F (see Figure S83 in SI).

In conclusion, through precise calculations of the electronic and vibrational properties, our study has revealed that hydrogen adsorption at the bridge site of β_{12} borophene not only ensures dynamical stability of the material but also preserves its intrinsic superconducting properties, characterized by a T_c of 6.3 K, as obtained from anisotropic Migdal-Eliashberg calculations. Moreover, this borophane system is prone to strong enhancement of the T_c through tensile strain or hole doping, in contrast to the bare borophene phase, and stands out among other borophane phases for its promising superconducting characteristics. As a concrete example, we showed that applying uniaxial tensile strain of 5% along the hydrogenated bridges increases the T_c to 28.6 K, above the liquid hydrogen temperature (20.3 K), making future practical applications more viable. This increase goes hand in hand with the increasing contribution at the E_F of the B-σ and the B-p_z states, with a minor contribution from the hybridized B-p_z/H-s state. This further highlights the crucial role of both B-σ and B-p_z states in governing superconductivity, contrasting the bare phase where σ states are predominant. We have also shown that similarly elevated T_c values can be achieved by moderate hole doping, but this effect is not additive to the one of the strain. With such

robust superconductivity and electronic and mechanical sensitivity, while also being more stable in ambient environments than its bare counterpart, our findings promote hydrogenated β_{12} borophene as a highly promising platform for further development of boron-based 2D superconducting technologies.

Acknowledgement

B.N.Š. acknowledges support from the Montenegrin Ministry of Science and the Special Research Fund of the University of Antwerp (BOF-UA) – No. 542300011. J.B. acknowledges support as a Senior Postdoctoral Fellow of Research Foundation-Flanders (FWO) under Fellowship No. 12ZZ323N. The computational resources and services were provided by the Flemish Supercomputer Center (VSC), funded by the FWO and the Flemish Government – department EWI. Our collaboration was fostered by EU-COST actions NANOCOHYBRI (Grant No. CA16218), SUPERQUMAP (Grant No. CA21144) and Hi-SCALE (Grant No. CA19108). The authors also thank D. Šabani and T. Pandey for fruitful discussions.

Supporting Information Available

In the Supporting Information (SI) we provide computational details, as well as our complete set of results on the electronic, vibrational, and superconducting properties of all considered compounds.

References

(1) Ogitsu, T.; Gygi, F.; Reed, J.; Motome, Y.; Galli, G. Imperfect Crystal and Unusual Semiconductor: Boron, a Frustrated Element. *Journal of the American Chemical Society* **2009**, *131*, 1903–1909.

(2) Sun, X.; Liu, X.; Yin, J.; Yu, J.; Li, Y.; Yang, H.; Zhou, X.; Yu, M.; Li, J.; Tai, G.;

Guo, W. Two-Dimensional Boron Crystals: Structural Stability, Tunable Properties, Fabrications and Applications. *Advanced Functional Materials* **2017**, *27*, 1603300.

(3) Oganov, A. R.; Solozhenko, V. L. Boron: a hunt for superhard polymorphs. *Journal of Superhard Materials* **2009**, *31*, 285–291.

(4) Boustani, I. Structure and stability of small boron clusters. A density functional theoretical study. *Chemical Physics Letters* **1995**, *240*, 135–140.

(5) Liu, Y.; Penev, E. S.; Yakobson, B. I. Probing the Synthesis of Two-Dimensional Boron by First-Principles Computations. *Angewandte Chemie International Edition* **2013**, *52*, 3156–3159.

(6) Zhang, Z.; Yang, Y.; Gao, G.; Yakobson, B. I. Two-Dimensional Boron Monolayers Mediated by Metal Substrates. *Angewandte Chemie International Edition* **2015**, *54*, 13022–13026.

(7) Mannix, A. J.; Zhou, X. F.; Kiraly, B.; Wood, J. D.; Alducin, D.; Myers, B. D.; Liu, X.; Fisher, B. L.; Santiago, U.; Guest, J. R.; Yacaman, M. J.; Ponce, A.; Oganov, A. R.; Hersam, M. C.; Guisinger, N. P. Synthesis of borophenes: Anisotropic, two-dimensional boron polymorphs. *Science* **2015**, *350*, 1513–1516.

(8) Feng, B.; Zhang, J.; Zhong, Q.; Li, W.; Li, S.; Li, H.; Cheng, P.; Meng, S.; Chen, L.; Wu, K. Experimental realization of two-dimensional boron sheets. *Nature chemistry* **2016**, *8*, 563–568.

(9) Penev, E. S.; Bhowmick, S.; Sadrzadeh, A.; Yakobson, B. I. Polymorphism of two-dimensional boron. *Nano letters* **2012**, *12*, 2441–2445.

(10) Kiraly, B.; Liu, X.; Wang, L.; Zhang, Z.; Mannix, A. J.; Fisher, B. L.; Yakobson, B. I.; Hersam, M. C.; Guisinger, N. P. Borophene Synthesis on Au(111). *ACS Nano* **2019**, *13*, 3816–3822.

(11) Wu, R.; Drozdov, I. K.; Eltinge, S.; Zahl, P.; Ismail-Beigi, S.; Božović, I.; Gozar, A. Large-area single-crystal sheets of borophene on Cu(111) surfaces. *Nature Nanotechnology* **2019**, *14*, 44–49.

(12) Vinogradov, N. A.; Lyalin, A.; Taketsugu, T.; Vinogradov, A. S.; Preobrajenski, A. Single-Phase Borophene on Ir(111): Formation, Structure, and Decoupling from the Support. *ACS Nano* **2019**, *13*, 14511–14518.

(13) Radatović, B.; Jadriško, V.; Kamal, S.; Kralj, M.; Novko, D.; Vujičić, N.; Petrović, M. Macroscopic Single-Phase Monolayer Borophene on Arbitrary Substrates. *ACS Applied Materials & Interfaces* **2022**, *14*, 21727–21737.

(14) Ranjan, P.; Sahu, T. K.; Bhushan, R.; Yamijala, S.; Late, D. J.; Kumar, P.; Vinu, A. Freestanding Borophene and Its Hybrids. *Advanced Materials* **2019**, *31*, 1900353.

(15) Zhang, Z.; Yang, Y.; Penev, E. S.; Yakobson, B. I. Elasticity, Flexibility, and Ideal Strength of Borophenes. *Advanced Functional Materials* **2017**, *27*, 1605059.

(16) Zhang, Z.; Mannix, A. J.; Hu, Z.; Kiraly, B.; Guisinger, N. P.; Hersam, M. C.; Yakobson, B. I. Substrate-Induced Nanoscale Undulations of Borophene on Silver. *Nano Letters* **2016**, *16*, 6622–6627.

(17) Adamska, L.; Sadasivam, S.; Foley, J. J. I.; Darancet, P.; Sharifzadeh, S. First-Principles Investigation of Borophene as a Monolayer Transparent Conductor. *The Journal of Physical Chemistry C* **2018**, *122*, 4037–4045.

(18) Er, S.; de Wijs, G. A.; Brocks, G. DFT Study of Planar Boron Sheets: A New Template for Hydrogen Storage. *The Journal of Physical Chemistry C* **2009**, *113*, 18962–18962.

(19) Li, X.; Tan, X.; Xue, Q.; Smith, S. Charge-controlled switchable H2 storage on conductive borophene nanosheet. *International Journal of Hydrogen Energy* **2019**, *44*, 20150–20157.

(20) Liu, T.; Chen, Y.; Wang, H.; Zhang, M.; Yuan, L.; Zhang, C. Li-Decorated β_{12}-Borophene as Potential Candidates for Hydrogen Storage: A First-Principle Study. *Materials* **2017**, *10*.

(21) Xiao, H.; Cao, W.; Ouyang, T.; Guo, S.; He, C.; Zhong, J. Lattice thermal conductivity of borophene from first principle calculation. *Scientific Reports* **2017**, *7*, 45986.

(22) Feng, B. et al. Dirac Fermions in Borophene. *Physical Review Letters* **2017**, *118*, 096401.

(23) Feng, B.; Zhang, J.; Ito, S.; Arita, M.; Cheng, C.; Chen, L.; Wu, K.; Komori, F.; Sugino, O.; Miyamoto, K.; Okuda, T.; Meng, S.; Matsuda, I. Discovery of 2D Anisotropic Dirac Cones. *Advanced Materials* **2018**, *30*, 1704025.

(24) Penev, E. S.; Kutana, A.; Yakobson, B. I. Can Two-Dimensional Boron Superconduct? *Nano Letters* **2016**, *16*, 2522–2526.

(25) Zhao, Y.; Zeng, S.; Lian, C.; Dai, Z.; Meng, S.; Ni, J. Multigap anisotropic superconductivity in borophenes. *Physical Review B* **2018**, *98*, 134514.

(26) Šoškić, B. N.; Bekaert, J.; Sevik, C.; Šljivančanin, Z.; Milošević, M. V. First-principles exploration of superconductivity in intercalated bilayer borophene phases. *Phys. Rev. Mater.* **2024**, *8*, 064803.

(27) Jiang, H.; Lu, Z.; Wu, M.; Ciucci, F.; Zhao, T. Borophene: A promising anode material offering high specific capacity and high rate capability for lithium-ion batteries. *Nano Energy* **2016**, *23*, 97–104.

(28) Singh, Y.; Back, S.; Jung, Y. Computational exploration of borophane-supported single transition metal atoms as potential oxygen reduction and evolution electrocatalysts. *Physical Chemistry Chemical Physics* **2018**, *20*, 21095–21104.

(29) Nagarajan, V.; Chandiramouli, R. Borophene nanosheet molecular device for detection

of ethanol – A first-principles study. *Computational and Theoretical Chemistry* **2017**, *1105*, 52–60.

(30) Shen, J.; Yang, Z.; Wang, Y.; Xu, L.-C.; Liu, R.; Liu, X. The gas sensing performance of borophene/MoS2 heterostructure. *Applied Surface Science* **2020**, *504*, 144412.

(31) Alvarez-Quiceno, J. C.; Miwa, R. H.; Dalpian, G. M.; Fazzio, A. Oxidation of free-standing and supported borophene. *2D Materials* **2017**, *4*, 025025.

(32) Lei, X.; Zatsepin, A. F.; Boukhvalov, D. W. Chemical instability of free-standing boron monolayers and properties of oxidized borophene sheets. *Physica E: Low-dimensional Systems and Nanostructures* **2020**, *120*, 114082.

(33) Mu, Y.; Li, S. D. First-Principles Study on the Oxidation of Supported β_{12}-Borophene. *The Journal of Physical Chemistry C* **2020**, *124*, 28145–28151.

(34) Lyding, J. W.; Shen, T.-C.; Hubacek, J. S.; Tucker, J. R.; Abeln, G. C. Nanoscale patterning and oxidation of H-passivated Si(100)-2×1 surfaces with an ultrahigh vacuum scanning tunneling microscope. *Applied Physics Letters* **1994**, *64*, 2010–2012.

(35) Qiu, J.; Fu, H.; Xu, Y.; Oreshkin, A. I.; Shao, T.; Li, H.; Meng, S.; Chen, L.; Wu, K. Ordered and Reversible Hydrogenation of Silicene. *Physical Review Letters* **2015**, *114*, 126101.

(36) Bianco, E.; Butler, S.; Jiang, S.; Restrepo, O. D.; Windl, W.; Goldberger, J. E. Stability and Exfoliation of Germanane: A Germanium Graphane Analogue. *ACS Nano* **2013**, *7*, 4414–4421.

(37) Li, Q.; Kolluru, V. S. C.; Rahn, M. S.; Schwenker, E.; Li, S.; Hennig, R. G.; Darancet, P.; Chan, M. K. Y.; Hersam, M. C. Synthesis of borophane polymorphs through hydrogenation of borophene. *Science* **2021**, *371*, 1143–1148.

(38) Drozdov, A. P.; Eremets, M. I.; Troyan, I. A.; Ksenofontov, V.; Shylin, S. I. Conventional superconductivity at 203 kelvin at high pressures in the sulfur hydride system. *Nature* **2015**, *525*, 73–76.

(39) Somayazulu, M.; Ahart, M.; Mishra, A. K.; Geballe, Z. M.; Baldini, M.; Meng, Y.; Struzhkin, V. V.; Hemley, R. J. Evidence for Superconductivity above 260 K in Lanthanum Superhydride at Megabar Pressures. *Physical Review Letters* **2019**, *122*, 027001.

(40) Drozdov, A. P.; Kong, P. P.; Minkov, V. S.; Besedin, S. P.; Kuzovnikov, M. A.; Mozaffari, S.; Balicas, L.; Graf, F. F. B. D. E.; Prakapenka, V. B.; Greenberg, E.; Knyazev, D. A.; Tkacz, M.; Eremets, M. I. Superconductivity at 250 K in lanthanum hydride under high pressures. *Nature* **2019**, *569*, 528–531.

(41) Ashcroft, N. W. Metallic Hydrogen: A High-Temperature Superconductor? *Physical Review Letters* **1968**, *21*, 1748–1749.

(42) Azadi, S.; Monserrat, B.; Foulkes, W. M. C.; Needs, R. J. Dissociation of High-Pressure Solid Molecular Hydrogen: A Quantum Monte Carlo and Anharmonic Vibrational Study. *Physical Review Letters* **2014**, *112*, 165501.

(43) McMinis, J.; Clay, R. C.; Lee, D.; Morales, M. A. Molecular to Atomic Phase Transition in Hydrogen under High Pressure. *Physical Review Letters* **2015**, *114*, 105305.

(44) Bekaert, J.; Petrov, M.; Aperis, A.; Oppeneer, P. M.; Milošević, M. V. Hydrogen-Induced High-Temperature Superconductivity in Two-Dimensional Materials: The Example of Hydrogenated Monolayer MgB_2. *Physical Review Letters* **2019**, *123*, 077001.

(45) Bekaert, J.; Sevik, C.; Milošević, M. V. Enhancing superconductivity in MXenes through hydrogenation. *Nanoscale* **2022**, *14*, 9918–9924.

(46) Petrov, M.; Bekaert, J.; Milošević, M. V. Superconductivity in gallenene. *2D Materials* **2021**, *8*, 035056.

(47) Meninno, A.; Errea, I. Absence of sizable superconductivity in hydrogen boride: A first-principles study. *Physical Review B* **2022**, *106*, 214508.

(48) Li, X.; Kutana, A.; Penev, E. S.; Yakobson, B. I. Limits of Hydrogen-Boosted Superconductivity in Borophene. *The Journal of Physical Chemistry C* **2024**, *128*, 483–488.

(49) Bekaert, J.; Aperis, A.; Partoens, B.; Oppeneer, P. M.; Milošević, M. V. Evolution of multigap superconductivity in the atomically thin limit: Strain-enhanced three-gap superconductivity in monolayer MgB_2. *Phys. Rev. B* **2017**, *96*, 094510.